JOURNAL OF GEOPHYSICAL RESEARCH, VOL. 96, NO. A10, PAGES 17,827–17,838, OCTOBER 1, 1991

Measurements of Ionospheric and Thermospheric Temperatures and Densities With the Middle and Upper Atmosphere Radar

WILLIAM L. OLIVER,[1,2] TOMOYUKI TAKAMI,[1] SHOICHIRO FUKAO,[1] TORU SATO,[3] MAMORU YAMAMOTO,[1] TOSHITAKA TSUDA,[1] TAKUJI NAKAMURA,[1] AND SUSUMU KATO[1]

The first incoherent scatter radar local time/seasonal/solar cycle averages of F region electron, ion, and neutral temperatures for Asian longitudes are presented. These measurements were made with the four-pulse experiment by the middle and upper atmosphere (MU) radar in Japan over the period August 1986 to April 1990. The neutral temperature and density results are compared with MSIS-86 model predictions. We divide our data into low and high solar activity levels, four seasons, and 24 one-hour times bins. While the seasonal and solar activity behavior of the ionospheric density, and of the anticorrelation of the electron temperature with this density, shows many aspects in common with those at other locations, a few particular differences are evident. At low solar activity the height of the F layer varies from 240 km during the day to 320 km at night, regardless of season. At high solar activity the maximum density of the F layer varies little with season. These facts seem to indicate little seasonal change in F region neutral atmospheric composition at this geographic location. At solar maximum the F layer is established at a higher altitude than at low solar activity, and the summer F layer in particular is formed at such a high altitude that its decay at night is very slow, its diurnal variation is hence weak, and the density remains so high at sunrise that little sunrise effect in the electron temperature is produced. The neutral temperatures in the F region have the same basic diurnal pattern as does the MSIS-1986 model temperatures, but the radar temperatures are consistently lower by an amount ranging up to 160 K for summer conditions at high solar activity. The measured and model temperatures are closest in the autumn and winter. The neutral density results are of low quality and do not provide any evidence of need to modify the MSIS model densities.

1. INTRODUCTION

The Japanese middle and upper atmosphere (MU) radar (34.85°N, 136.10°E) is the newest of the large atmospheric radars capable of detecting the incoherent scatter (IS) from the free electrons in the ionosphere. This radar system has been described by *Fukao et al.* [1985*a*, *b*]. *Sato et al.* [1989] have discussed the capability and the techniques used for IS observations with this radar. IS observations began in December 1985, and several scientific studies with these data have been published starting in 1988. *Oliver et al.* [1988*a*], *Fukao et al.* [1991*b*], and *Reddy et al.* [1990*a*, *b*] have reported on F region electrodynamics; *Oliver et al.* [1988*b*] and *Oliver and Hagan* [1991] have reported on F region gravity waves; *Fukao et al.* [1988, 1991*a*], *Kelley and Fukao* [1991], and *Yamamoto et al.* [1991] have reported on ionospheric irregularities; and *Saryo et al.* [1989*a*, *b*] and *Oliver et al.* [1990] have reported on thermospheric winds.

In the current paper we use the data from 29 experiments covering 55 whole or partial days during the period August 11, 1986, to April 26, 1990, to determine the average solar activity, seasonal, and time-of-day behavior of the ionospheric temperatures and density over the MU radar, and then we use these averaged results to deduce the behavior of the neutral atmosphere temperature and density.

[1]Radio Atmospheric Science Center, Kyoto University, Kyoto, Japan.
[2]Department of Electrical, Computer and Systems Engineering Boston University, Boston, Massachusetts.
[3]Department of Electrical Engineering II, Kyoto University, Kyoto, Japan.

Paper number 91JA01654.
0148-0227/91/91JA-01654$05.00

2. THE DATA

Fukao et al. [1985*a*, *b*] have discussed the MU radar system, and *Sato et al.* [1989] have discussed its sensitivity for IS measurements. As discussed by Sato et al., different MU radar experiments are used for different measurable quantities.

Power profile measurements, from which the electron density profile may be computed, are generally made with a 7-bit Barker-coded pulse having a 64-μs subpulse width, or 9.6-km range resolution. The received power profile is corrected for range dependence and normalized according to F layer peak-density information obtained with an on-site ionosonde to produce the electron density profile.

Plasma temperatures are measured normally with a four-pulse experiment using a 96-μs subpulse width. This waveform provides a 14.4-km range resolution and 6 points on the signal autocorrelation function (acf) evenly spaced from 192 to 1152 μs lag. The correlation time of the scattering medium is of the order of 1 ms in the F region at the MU radar frequency, so such a long waveform is required to provide adequate spectral resolution. The length of the entire transmitted waveform is 1248 μs, and, including a required guard time between antenna transmission and reception of 74 μs, this results in a lowest possible observable range of 198.2 km. Other waveforms with superior spectral resolution are possible, but the price paid is an even higher initial height of measurement.

The measured acf's are analyzed to provide estimates of the ion and electron temperatures through comparison with a library of theoretical acf's. The ions are assumed to be O^+ except in the region below 270 km altitude, where a specific height-dependent mixture of O^+, NO^+, and O_2^+ ions is assumed, but the molecular ions become important for the analysis only below 230 km.

MU radar IS experiments designed for temperature measurement normally use a cycle time of 1 hour, combining a

TABLE 1. MU Radar Four-Pulse Temperature Experiments

Year	Start Date	Start Time	End Date	End Time	Hours	$F_{10.7}$	Ap
1986	Aug. 11	0930	Aug. 16	0900	73	69 68 68 68 70 69	7 10 10 5 6 4
	Sept. 16	0415	Sept. 17	0800	20	70 69	7 14
	Nov. 5	1430	Nov. 06	1900	20	82 81	20 12
	Dec. 14	0515	Dec. 16	1300	38	71 71 71	20 4 12
1987	Aug. 26	0015	Aug. 27	2400	32	87 85	40 21
	Sept. 21	1215	Sept. 22	1700	20	83 81	10 29
	Sept. 24	0815	Sept. 25	1700	23	80 78	14 46
1988	Jan. 25	0900	Jan. 26	1700	24	95 94	6 8
	March 19	0030	March 22	0830	57	116 116 118 118	4 6 2 3
	June 13	2022	June 13	2059	1	115	6
	June 14	0415	June 14	0500	1	112	20
	June 14	2015	June 14	2100	1	112	20
	June 15	0415	June 15	0500	1	114	9
	July 13	0015	July 13	0100	1	141	10
	July 13	1715	July 13	1800	1	141	10
	July 14	0315	July 14	0400	1	150	15
	July 14	1215	July 14	1300	1	150	15
	Dec. 03	1500	Dec. 04	0145	8	147 143	18 10
1989	April 12	1230	April 13	1600	17	181 185	6 17
	May 10	1215	May 11	1300	17	209 199	4 6
	May 31	1230	June 02	1600	37	194 192 208	13 11 19
	Aug. 03	1225	Aug. 04	1300	17	220 226	5 8
	Oct. 04	1215	Oct. 05	2230	22	234 223	6 5
	Nov. 29	1215	Nov. 30	1300	18	215 241	19 20
	Dec. 14	1715	Dec. 15	1600	17	162 166	12 10
1990	Jan. 25	1615	Jan. 26	1200	15	235 239	19 10
	Feb. 21	1315	Feb. 22	1145	6	212 216	16 21
	March 21	1215	March 22	1200	17	228 243	76 28
	April 25	1815	April 26	1800	18	198 189	19 16

15-min density measurement with a 45-min temperature measurement. Data are recorded on tape at much more frequent intervals, but the normal analysis employed on these data postintegrates the power data to a single 15-min average and the acf data to a single 45-min average for each cycle. These normal data collection and analysis schemes were used to analyze all data reported in this paper. Radar receiver samples are collected at 32-μs intervals in these experiments. For our current analysis we have postintegrated every 10 range gates into a single data record, producing 45-km height resolution. As the times of the temperature and density measurements are interlaced, their center times differ by $\frac{1}{2}$ hour. For our presentations in this paper we have interpolated the density measurements to the times of the temperature measurements. The data then all apply to local solar times of 0.7, 1.7, 2.7, ···, 22.7, 23.7 hours. We also note that we have corrected the collective electron scattering cross section for its dependence on the ratio T_e/T_i, so that the densities determined from the power measurements are true estimates of the electron density.

3. Ionospheric Temperature and Density Measurements

We have available for our study hourly measurements of the altitude profiles of the ion temperature T_i, the electron temperature T_e, and the electron density $[e]$ from 29 experiments covering all or parts of 55 different days during the period August 11, 1986, to April 26, 1990. Table 1 lists these experiments and gives the solar 10.7-cm flux index $F_{10.7}$ and the daily geomagnetic Ap index for each day of measurement. $F_{10.7}$ ranged from 68 to 243 units during the period, encompassing essentially the entire range of a solar cycle, while Ap ranged from 2 to 76, with only 5 days (82 hours of data) experiencing values above 21. As the ionospheric conditions must be very different over this large range of solar activity, for averaging purposes we have separated the data into different solar activity groups. Because of our limited amount of data, we can only separate the data into two solar activity groups and maintain measurements in most seasons. We have chosen to separate the data into the sets 1986–1988 and 1989–1990 based on the large break point in the $F_{10.7}$ indices occurring at this point in time. We will call these the "low" and "high" solar activity periods. Their ranges of $F_{10.7}$ are 68–150 for low activity and 162–243 for high activity, and the midpoints of these ranges are 109 and 202.

For each solar activity period we further divide the data into four 3-month seasons, with winter defined as the period November 5 to February 4, spring as February 5 to May 6, summer as May 7 to August 4, and fall as August 5 to November 4. Thus we have eight groupings of data, and for each grouping we have computed an average altitude profile for each of T_i, T_e, and $[e]$ for each hour of the day. In Table 2 we list the number of data points in each solar activity/season/time bin. Clearly, our data population is very sparse, and characteristics of behavior on the individual days are highly likely to be evident in the averages. This is particularly true where there is a large population difference among

TABLE 2. Bin Populations

	Low Solar Activity				High Solar Activity				
Hour	Winter	Spring	Summer	Autumn	Winter	Spring	Summer	Autumn	Hour
00–01	5	4	0	4	3	2	3	1	00–01
01–02	5	4	0	4	3	2	4	1	01–02
02–03	4	4	0	4	3	2	4	1	02–03
03–04	4	4	0	4	3	2	4	1	03–04
04–05	3	4	2	4	3	1	4	1	04–05
05–06	4	4	0	3	3	2	4	1	05–06
06–07	5	4	0	4	3	1	1	1	06–07
07–08	5	3	0	4	3	2	4	1	07–08
08–09	3	2	0	5	3	2	4	1	08–09
09–10	5	2	0	5	3	2	4	0	09–10
10–11	6	3	0	5	3	2	4	1	10–11
11–12	6	3	0	5	3	1	4	1	11–12
12–13	5	3	0	6	2	1	6	1	12–13
13–14	4	3	0	6	2	2	4	1	13–14
14–15	6	2	0	5	2	2	4	1	14–15
15–16	6	2	0	6	2	2	5	1	15–16
16–17	6	3	0	5	2	1	4	2	16–17
17–18	6	3	0	3	3	2	3	2	17–18
18–19	6	3	0	3	3	2	4	2	18–19
19–20	4	3	0	4	3	2	4	2	19–20
20–21	5	3	2	4	3	2	4	2	20–21
21–22	5	3	0	4	3	2	4	2	21–22
22–23	5	3	0	4	3	2	3	1	22–23
23–24	5	3	0	4	3	2	3	1	23–24

the 24 time bins for a particular solar activity/season case, as this will mean that different individual experiments are contributing to different parts of the day, and systematic discontinuities in the averages are prone to occur in these cases. It is clear from Table 1 that many of the experiments give partial-day records. Certainly, our averages will become smoother as we incorporate future data. We considered sorting our data into 4-month solstices and 2-month equinoxes, in recognition of predictions of rapid equinox transitions, but the sparseness of our data prevented the adoption of the shorter seasons. We display the averages for our 29 experiments in Figure 1 in the form of 32 time-height contour plots. For each of these eight groups we have computed the mean day number, mean solar index, and mean magnetic index for the data in the group. These results are given in Table 3. We have few data for low solar activity summer conditions; thus we will not discuss this case.

In Figure 2 we display the F layer maximum density N_{max} and the height of this maximum density h_{max} to correspond with the $[e]$ contour plots of Figure 1 to facilitate our discussion of these results.

4. Neutral Temperature and Density Results

Bauer et al. [1970] developed a procedure by which we may estimate the F region neutral temperature T_n and neutral density from knowledge of the F region ionospheric temperatures and densities. This method is well established, and we will not discuss its basis here, but a few comments on this method will help to explain some characteristics of the results shown below. T_n has approached its asymptotic exospheric value T_∞ by the time we ascend to 300 km altitude, and at this altitude the ions are strongly thermally tied to the neutrals, so that T_i itself in this region is a good measure of T_∞. As we ascend higher in altitude, T_i begins to depart from T_n as the neutral density diminishes, and T_i eventually approaches T_e. It is the height gradient of this departure of T_i from T_n that gives us a measure of the neutral density. As we are here trying to measure a gradient of T_i instead of its value, and because the region of the gradient is at a higher altitude of lower signal strength, we find that the uncertainty in the measurement of the neutral density is much greater than the uncertainty in the measurement of T_n. The unfortunate result for our current study is that even when we average all of our data irrespective of solar activity and season, the error bars on the resulting neutral density versus time-of-day plot cover the entire range of daily neutral density variation expected from current models (the MSIS-1986 model of *Hedin* [1987]), and hence we have no evidence that the model values are not good estimates. Because of this we have chosen to redo our data analysis using the MSIS-1986 model neutral densities and determining only T_∞. We do show below, for completeness, the neutral density determination mentioned above, in the form of the neutral atomic oxygen density referenced to 400 km altitude (atomic oxygen predominates at these altitudes).

Applying the aforementioned procedure to the ionospheric data shown in Figure 1 gives the T_∞ results shown in Figure 3. Included are MSIS-86 model values for comparison, where the day number and solar-geophysical parameters used as inputs to the model are those listed in Table 3. The full MSIS-86 model requires the three-solar-rotation average plus the prior-day value as solar flux inputs and a recent history of 3-hour *ap* indices for prediction of instantaneous conditions. We have not used this complication for our case

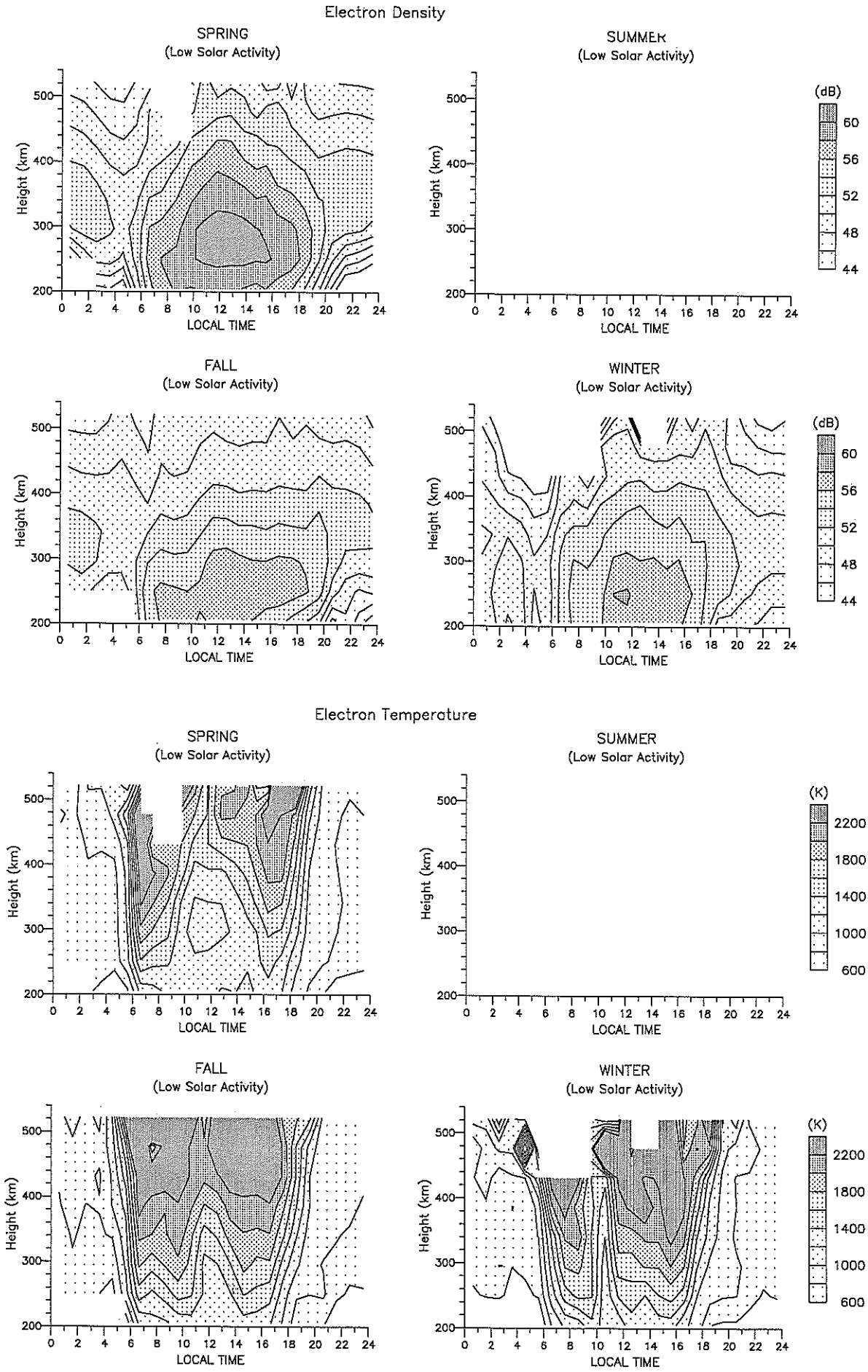

Fig. 1. The MU radar $[e]$, T_e, $T_r = T_e/T_i$, and T_i data averaged into two solar activity periods and four seasons. The density dB unit is equivalent to 10 log $[e]$ with $[e]$ in units of cm^{-3}.

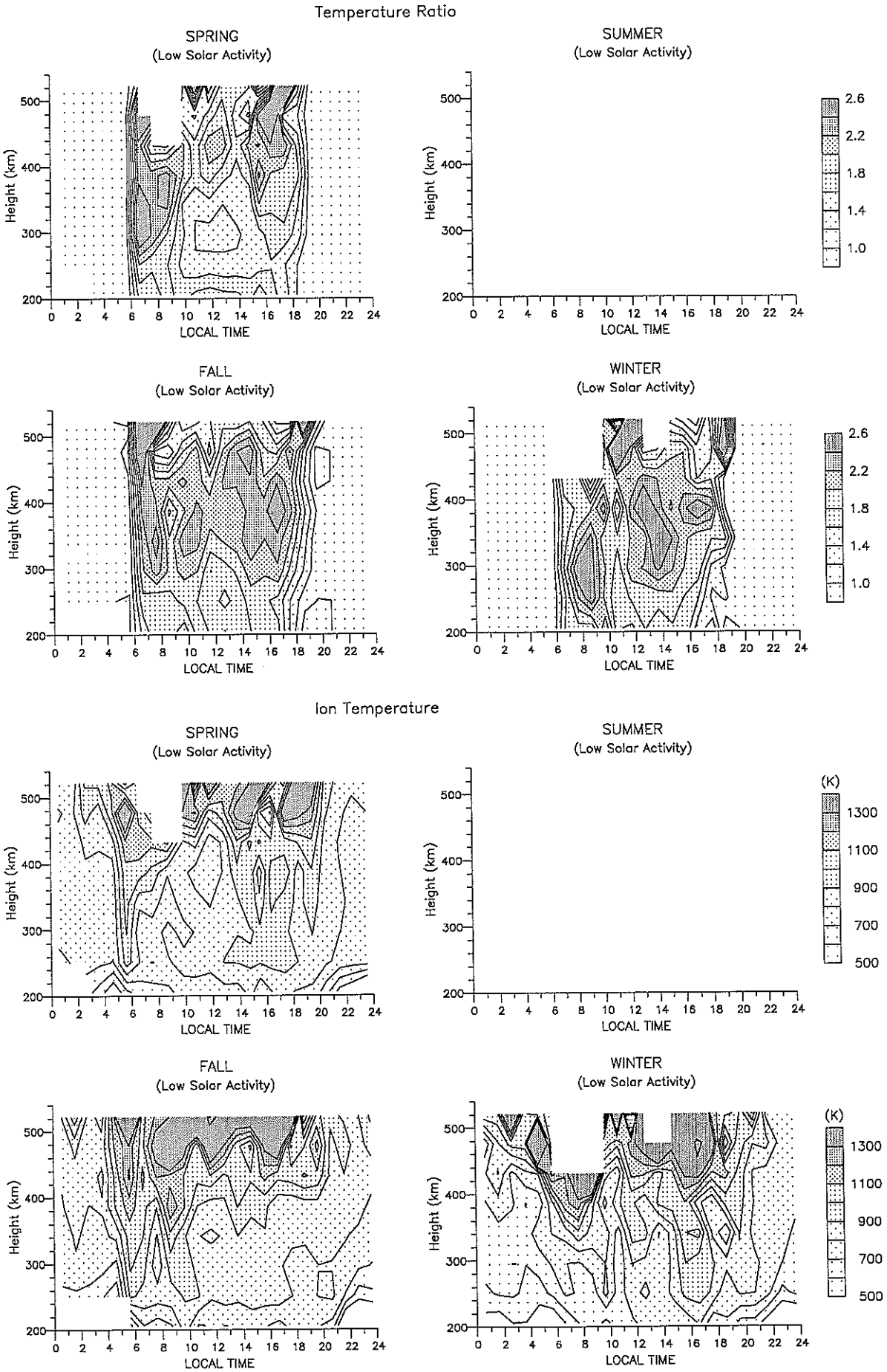

Fig. 1. (continued)

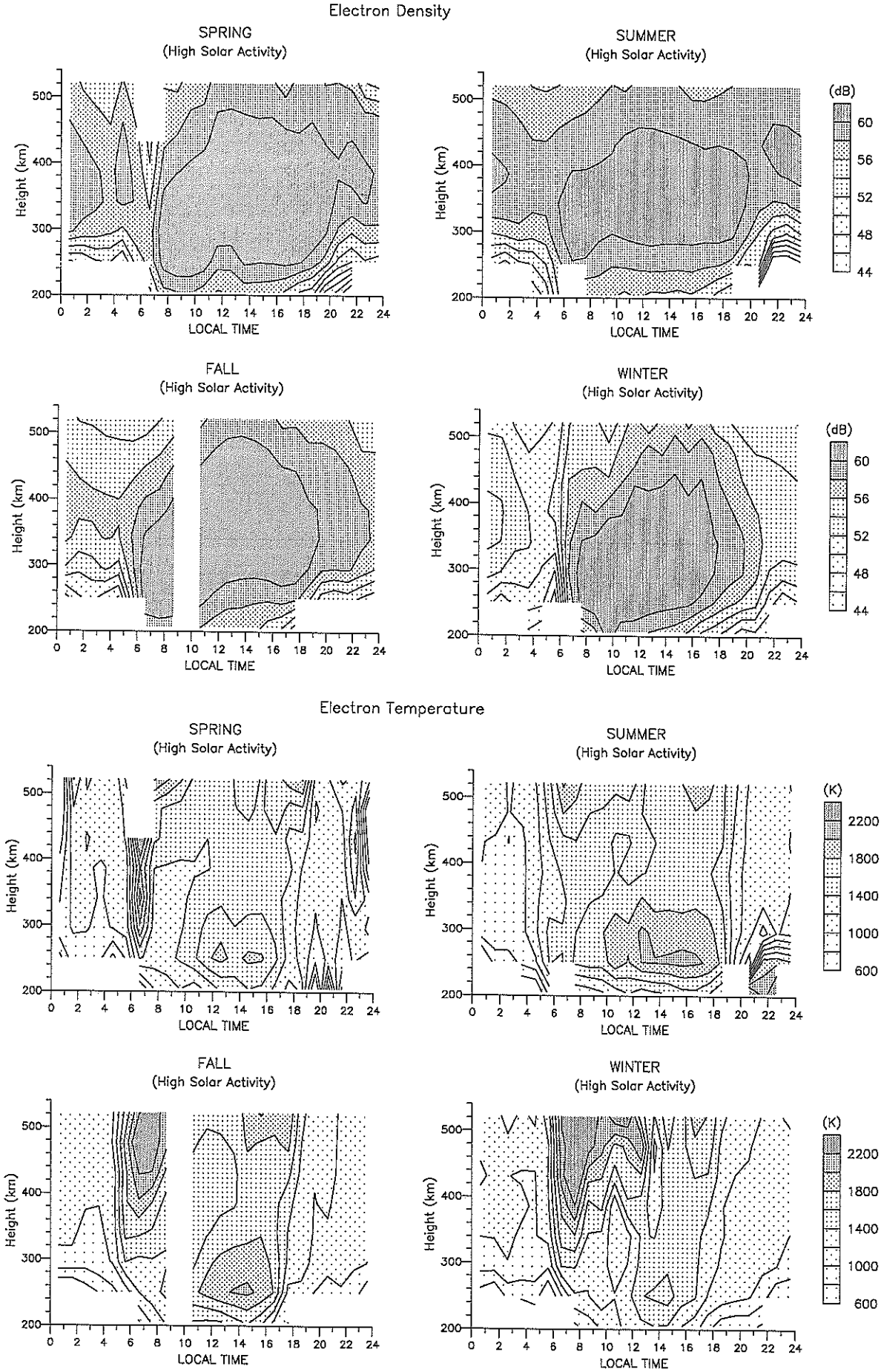

Fig. 1. (continued)

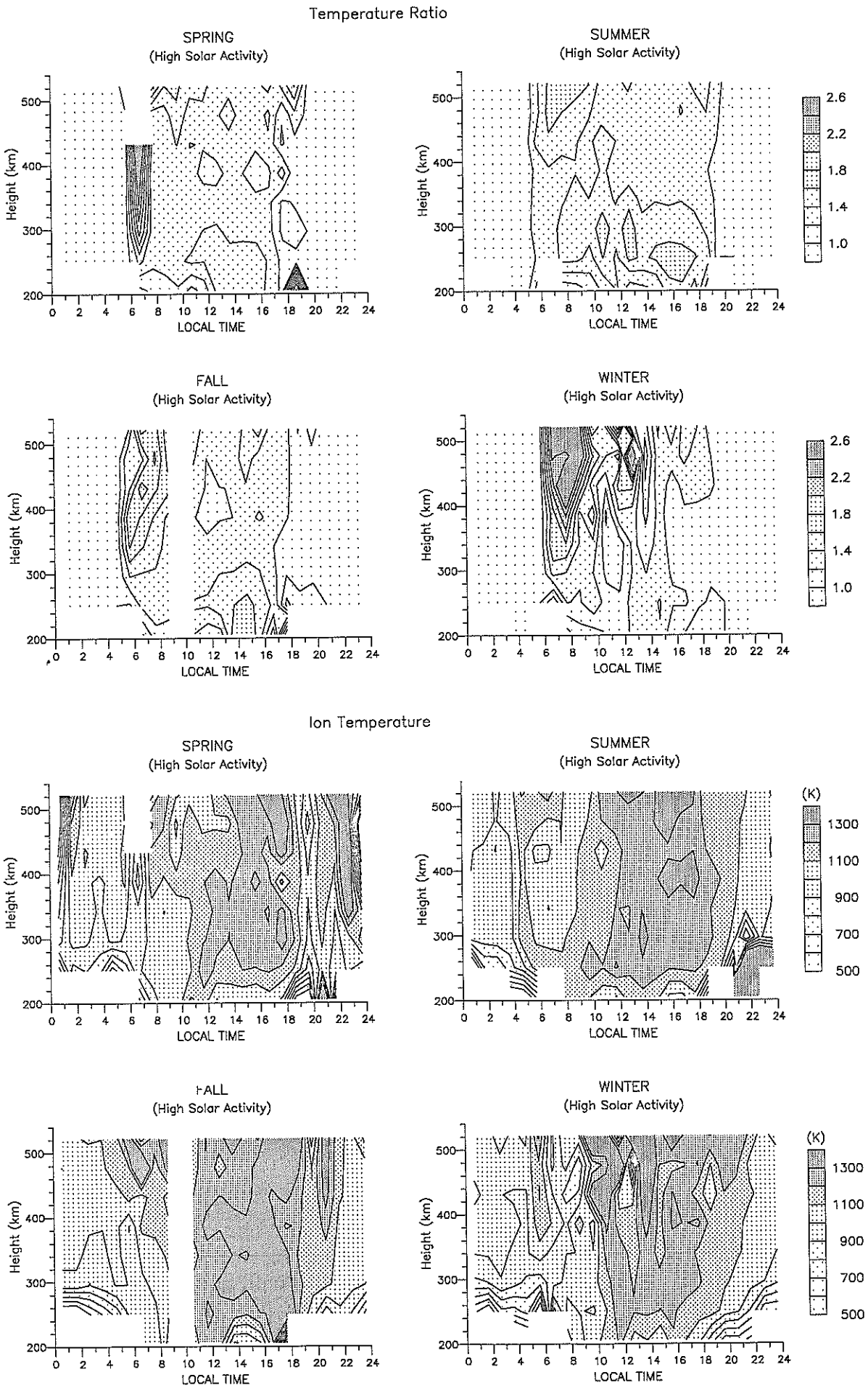

Fig. 1. (continued)

TABLE 3. Mean Day, $F_{10.7}$, Ap, and Model-Minus-Data Values for the Solar Activity and Seasonal Groupings

	Low Solar Activity				High Solar Activity			
	Winter	Spring	Summer	Autumn	Winter	Spring	Summer	Autumn
Day	Dec. 14	March 22	June 6	Sept. 17	Dec. 24	March 19	June 16	Oct. 06
$F_{10.7}$	97	118	114	82	218	203	211	223
Ap	10	2	9	25	13	19	11	5
$T_{model} - T_{data}$	46	79		3	35	114	158	65

$T_{model} - T_{data}$ is the daily median difference between the MSIS-1986 model and the MU radar data T_∞ values.

of averaged data but rather have opted to consider that the average-condition values in Table 3 are adequate for our current purposes.

5. Discussion of the Results

We begin by discussing the ionospheric density and temperature results. First, for low solar activity we must be careful to recognize that there is a correlation between season and solar activity in our data, as shown in Table 3. Of the three seasons for which we have data, spring has the highest solar activity and autumn the lowest, and this order corresponds exactly with the maximum [e] observed during these seasons. Any seasonal variation in electron density is not distinguishable from the possible solar activity variation. The T_e plots show the expected close anticorrelation between T_e and [e], which basically relates to the number of electrons available to share the incoming energy of the solar ionizing radiation. There are basic patterns of T_e increases near sunrise and sunset, when the density is low but the Sun is shining. The decreases in T_e during the day relate to the timing and amplitude of the daytime [e] buildup, and the higher the density, the lower the temperature. T_e is higher at higher altitudes where [e] is lower. T_i is largely a "slave" parameter, being determined largely by considerations of collisional heat transfer with the electrons and neutrals, and we will only note here that T_i remains close to T_n at the lower altitudes of Figure 1 but shows clear evidence of departure toward T_e at higher altitudes. We discuss T_n in a later paragraph. The T_e/T_i ratio shows the same heating features as does T_e but with more temporal clarity at the sunrise-sunset terminator times.

The h_{max} and N_{max} plots of Figure 2 (still considering the low solar activity case) indicate some of the effects of dynamics on the [e] behavior. It is interesting that for all three seasons shown, h_{max} varies from a high of 360 km at night to a low of 240 km in the day; h_{max} may be expected to decrease at sunrise as the solar radiations penetrate to create a low daytime layer. We are surprised that h_{max} in winter drops to such a low level soon after midnight, clearly not in response to the Sun. The [e] at these postmidnight, predawn hours is very low. In fact, the h_{max} variations are very similar for the three seasons except for the predawn hours, when large differences exist. This seems to indicate very different seasonal dynamics during this time period, at least for the few days within our data base. h_{max} attains its lowest value of the day before noon. We have recognized and discussed this feature previously in relation to the behavior of the meridional neutral winds over the MU radar [*Oliver et al.*, 1990]. We noted there that, as it is ion drag which is the primary factor limiting the neutral wind speed, the neutral wind attains its greatest poleward value of the day before the ionosphere attains its large midday values. This large northward morning wind lowers the F layers to its lowest values of the day at this time. There is an interesting rise in h_{max} near 0400 LT in each season. Our previous electric field studies [*Fukao et al.*, 1991*b*] found no perturbation at this time of night which could lift the layer, but our neutral wind studies [*Oliver et al.*, 1990] did show a small, consistent, equatorward wind enhancement at this time, which would provide the lifting. This lifting is not accompanied by any peak density increase, so it would not seem to be associated with any production or plasmaspheric flux inputs. An alternative view of this phenomenon is that a postmidnight poleward wind prevails until about 0400 LT.

For high solar activity we have a much smaller variation between the average solar activity levels experienced during the four seasons. If we look at the N_{max} variations in Figure 2, we see that the greatest value of N_{max} reached during the day is very nearly the same for the four seasons, evidencing very little seasonal variation in the neutral atmosphere at this height and geographic location. But the minimum N_{max} reached during the predawn hours is very different between seasons, again indicating very different decay dynamics. In winter, N_{max} becomes very low, compared with the other seasons, as is the case for solar maximum. The summer N_{max} changes by a relatively small amount during the entire 24-hour day. Notice that h_{max} for this summer case remains high throughout the day and is especially high at night. At such high altitudes the nighttime decay is slow and the density remains at relatively high levels throughout the night. The effect of this high nighttime residual density is evident in the electron temperature behavior at sunrise, as we see here very little sunrise effect. The other seasons at high solar activity show strong sunrise effects exactly in those height-time areas of the contour maps at which the density is low. As is the case for low solar activity, h_{max} reaches its daily minimum level before noon.

In a previous study [*Fukao et al.*, 1991*a*] we presented [e] measurements for the low solar activity period June 1–5, 1987. No temperature data were taken during that experiment, so these data are not included here. But this experiment provides data to fill missing [e] data in Figure 1 for summer, low solar activity. The result of those data that we wish to note here is that for low solar activity summer conditions the [e] height profile by day consists of an F_2 region O^+ layer and an F_1 region NO^+/O_2^+ layer of similar peak densities. The competition for density dominance between these two layers controls the morphology of the

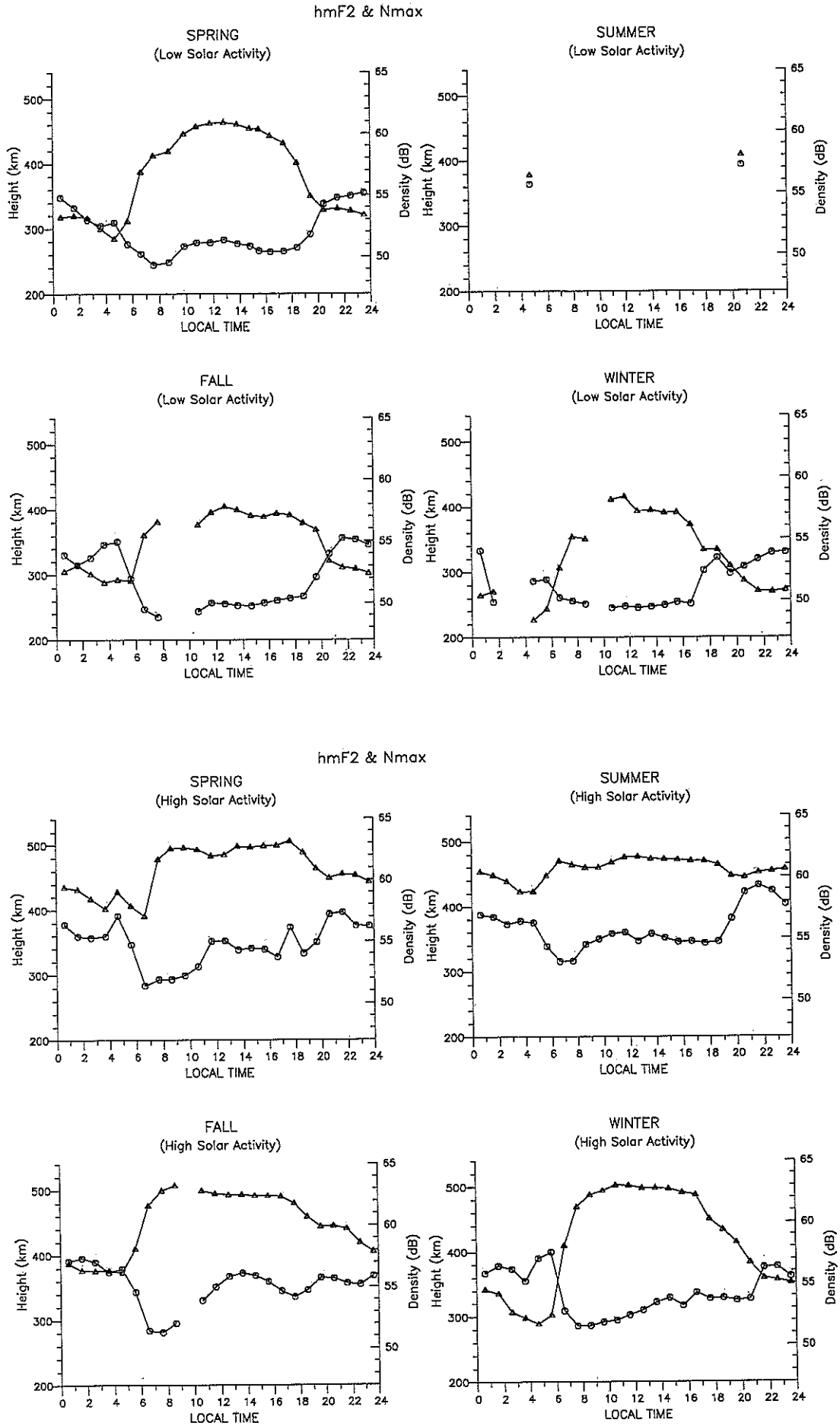

Fig. 2. Values of h_{max} (circles) and N_{max} (triangles) corresponding to the $[e]$ contours of Figure 1. The density dB unit is equivalent to 10 log $[e]$ with $[e]$ in units of cm^{-3}.

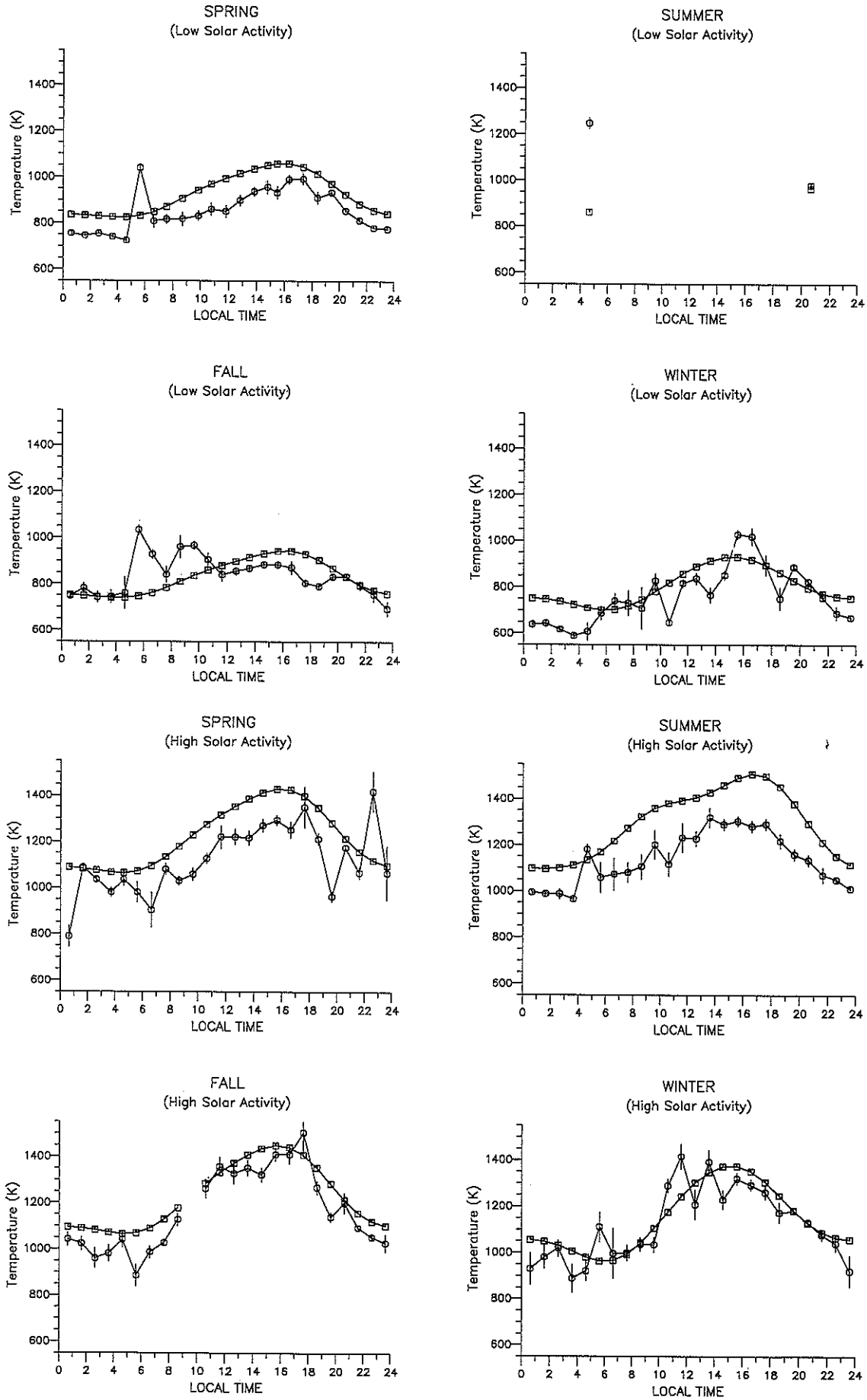

Fig. 3. T_∞ values deduced from the ionospheric averages of Figure 1: MSIS-86 model values (squares) and the MU radar data (circles).

composite F layer profile. Because these layers usually have comparable maximum densities, the layer shape is usually broad, and the height of peak density in the ionosphere is subject to large and sudden variation as one layer attains equal strength with the other. This competition no longer exists at high solar activity: the O^+ layer has risen and gained decided dominance while the molecular ion layer has moved little in comparison (it may be expected to fall slightly in altitude [see *Oliver*, 1979]). The seasonal shapes of the F region [e] profiles are much more alike at solar maximum than at solar minimum.

The ionospheric temperatures and densities just discussed all enter into the determination of the neutral temperature. These T_n results, shown in Figure 3, have diurnal behaviors resembling those of the MSIS-1986 model, and we will discuss here mainly the basic differences between the model and the data and the implications of these differences. The most outstanding difference is that the measured temperatures are consistently lower than the model temperatures. Those few periods for which this rule is not true appear to correspond to short-lived excursions of the measurements above the prevailing diurnal trend. The diurnal mean differences for our eight solar activity/season cases are listed in Table 3. These range from small values for autumn at low solar activity up to around 160 K for summer at high solar activity. This difference is consistently smaller during autumn and winter than during spring and summer. Another feature of the data is a tendency for temporary temperature enhancements to occur near sunrise. Our belief is that this is due to the sunrise effect itself, for at this time of day the ionospheric temperatures are changing rapidly with time; thus the ionospheric spectrum shape is changing rapidly with time, and our integration of data over 45 min thus results in the averaging of spectra of different shapes. This effectively smears out the spectral shape, which, in incoherent scatter spectral analysis, results in the deduction of an erroneously high value of T_i, and hence of T_n. There is, in fact, a high correlation between the times of positive perturbations of the temperature data in Figure 3 and periods of rapidly changing ionospheric temperatures in Figure 1. Were this rapid variability to be in truth the ionospheric behavior, then we would be liable to the aforementioned spectral smearing effects and temperature biases at these times. But we are more inclined not to take these cases too seriously at this time due to the sparseness of our data. Indeed, the autumn high solar activity case is largely just one day's measurement.

For completeness we show in Figure 4 the neutral atomic oxygen density at 400 km altitude ($[O]_{400}$) computed from the ionospheric data of Figure 1 after averaging these ionospheric data over the two solar activity levels and the four seasons. The poor quality of these results attests to the poor strength of the signal backscattered from the topside F region, from where this neutral composition information comes. Useful results are not possible at night, when T_n, T_i, and T_e are all equal. During the day the range of densities covered by the error bars includes the corresponding MSIS-1986 model density values about two thirds of the time, as would be expected statistically if the MSIS-1986 values were the true values. For this reason we have simply chosen to adopt the MSIS-1986 densities in our temperature computations.

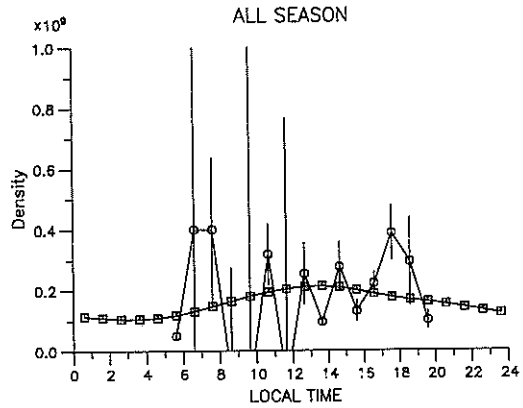

Fig. 4. $[O]_{400}(cm^{-3})$ deduced from averaging the ionospheric averages of Figure 1 over both solar activity and season: MSIS-86 model values (squares) and the MU radar data (circles).

Acknowledgments. The MU radar belongs to and is operated by the Radio Atmospheric Science Center of Kyoto University.

The Editor thanks A. E. Hedin and C. G. Fesen for their assistance in evaluating this paper.

REFERENCES

Bauer, P., P. Waldteufel, and D. Alcaydé, Diurnal variations of the atomic oxygen density and temperature determined from incoherent scatter measurements in the ionospheric F region, *J. Geophys. Res.*, *75*, 4825–4832, 1970.

Fukao, S., T. Sato, T. Tsuda, S. Kato, K. Wakasugi, and T. Makihara, The MU radar with an active phased array system, 1, Antenna and power amplifiers, *Radio Sci.*, *20*, 1155–1168, 1985*a*.

Fukao, S., T. Tsuda, T. Sato, S. Kato, K. Wakasugi, and T. Makihara, The MU radar with an active phased array system, 2, In-house equipment, *Radio Sci.*, *20*, 1169–1176, 1985*b*.

Fukao, S., J. P. McClure, A. Ito, T. Sato, I. Kimura, T. Tsuda, and S. Kato, First VHF radar observations of midlatitude F-region field-aligned irregularities, *Geophys. Res. Lett.*, *15*, 768–771, 1988.

Fukao, S., M. C. Kelley, T. Shirakawa, T. Takami, M. Yamamoto, T. Tsuda, and S. Kato, Turbulent upwelling of the mid-latitude ionosphere, 1, Observational results by the MU radar, *J. Geophys. Res.*, *96*, 3725–3746, 1991*a*.

Fukao, S., W. L. Oliver, Y. Onishi, T. Takami, T. Sato, T. Tsuda, M. Yamamoto, and S. Kato, F region seasonal behavior as measured by the MU radar, *J. Atmos. Terr. Phys.*, in press, 1991*b*.

Hedin, A. E., MSIS-86 thermospheric model, *J. Geophys. Res.*, *92*, 4649–4662, 1987.

Kelley, M. C., and S. Fukao, Turbulent upwelling of the mid-latitude ionosphere, 2, Theoretical framework, *J. Geophys. Res.*, *96*, 3747–3753, 1991.

Oliver, W. L., Incoherent scatter radar studies of the daytime middle thermosphere, *Ann. Geophys.*, *35*, 121–139, 1979.

Oliver, W. L., and M. E. Hagan, Simulation of a gravity wave observed by the MU radar, *J. Geophys. Res.*, *96*, 9793–9800, 1991.

Oliver, W. L., S. Fukao, T. Sato, T. Tsuda, S. Kato, I. Kimura, A. Ito, T. Saryou, and T. Araki, Ionospheric incoherent scatter measurements with the MU radar: Observations of F-region electrodynamics, *J. Geomagn. Geoelectr.*, *40*, 963–985, 1988*a*.

Oliver, W. L., S. Fukao, T. Sato, T. Tsuda, S. Kato, I. Kimura, A. Ito, T. Saryou, and T. Araki, Ionospheric incoherent scatter measurements with the middle and upper atmosphere radar: Observations during the large magnetic storm of February 6–8, 1986, *J. Geophys. Res.*, *93*, 14,649–14,655, 1988*b*.

Oliver, W. L., S. Fukao, T. Takami, M. Yamamoto, T. Tsuda, T. Nakamura, and S. Kato, Thermospheric meridional winds measured by the MU radar, *J. Geophys. Res.*, *95*, 7683–7692, 1990.

Reddy, C. A., S. Fukao, T. Takami, M. Yamamoto, T. Tsuda, T. Nakamura, and S. Kato, A MU radar–based study of mid-latitude

F region response to a geomagnetic disturbance, *J. Geophys. Res.*, *95*, 21,077–21,094, 1990*a*.

Reddy, C. A., A. Nishida, V. Y. Somayajulu, and S. Fukao, Magnetospheric substorm-related electric fields in the ionosphere: Discrepancy of an observation with model predictions, *Geophys. Res. Lett.*, *17*, 2333–2336, 1990*b*.

Saryo, T., M. Takeda, T. Araki, T. Sato, T. Tsuda, S. Fukao, and S. Kato, Ion drift measured by MU radar and its comparison with geomagnetic field variation, *J. Geomagn. Geoelectr.*, *41*, 597–611, 1989*a*.

Saryo, T., M. Takeda, T. Araki, T. Sato, T. Tsuda, S. Fukao, and S. Kato, A midday bite-out event of the *F*2-layer observed by the MU radar at Shigaraki, *J. Geomagn. Geoelectr.*, *41*, 727–734, 1989*b*.

Sato, T., A. Ito, W. L. Oliver, S. Fukao, T. Tsuda, S. Kato, and I. Kimura, Ionospheric incoherent scatter measurements with the middle and upper atmosphere radar: Techniques and capability, *Radio Sci.*, *24*, 85–98, 1989.

Yamamoto, M., S. Fukao, R. F. Woodman, T. Ogawa, T. Tsuda, and S. Kato, Mid-latitude *E* region field-aligned irregularities observed with the MU radar, *J. Geophys. Res.*, 15,943–15,949, 1991.

S. Fukao, S. Kato, T. Nakamura, T. Takami, T. Tsuda, and M. Yamamoto, Radio Atmospheric Science Center, Kyoto University, Uji, Kyoto 611, Japan.

W. L. Oliver, Department of Electrical, Computer and Systems Engineering, Boston University, 44 Cummington Street, Boston, MA 02215.

T. Sato, Department of Electrical Engineering II, Kyoto University, Kyoto 606, Japan.

(Received February 7, 1991;
revised June 17, 1991;
accepted June 18, 1991.)